International Journal of Solids and Structures 49 (2012) 2547–2558

Contents lists available at SciVerse ScienceDirect

International Journal of Solids and Structures

journal homepage: www.elsevier.com/locate/ijsolstr

Propagation of a mode-III interfacial crack in a piezoelectric–piezomagnetic bi-material

Hao-sen Chen [b], Wei-yi Wei [b], Jin-xi Liu [c,*], Dai-ning Fang [a,*]

[a] LTCS and College of Engineering, Peking University, Beijing 100871, China
[b] Department of Engineering Mechanics, Tsinghua University, Beijing 100084, China
[c] Department of Engineering Mechanics, Shijiazhuang Tiedao University, Shijiazhuang 050043, China

ARTICLE INFO

Article history:
Received 25 February 2012
Received in revised form 10 May 2012
Available online 31 May 2012

Keywords:
Dynamic fracture
Piezoelectric–piezomagnetic composite
Intensity factors
Universal functions
Bleustein–Gulyaev wave
Generalized Maerfeld–Tournois wave

ABSTRACT

The transient response of a semi-infinite mode-III interfacial crack propagating between piezoelectric (PE) and piezomagnetic (PM) half spaces is investigated in this paper. The integral transform method together with the Wiener–Hopf and Cagniard–de Hoop techniques is used to solve the mixed boundary value problem under consideration. The existence of generalized Maerfeld–Tournois interfacial wave is discussed and the solutions of the coupled fields are derived for four different cases of bulk shear wave velocity. The dynamic intensity factors of stress, electric displacement and magnetic induction as well as energy release rate (ERR) are obtained in explicit forms. The numerical results of the universal functions and dimensionless ERR for several different material combinations are presented and discussed in details. It is found that the Bleustein–Gulyaev (generalized Maerfeld–Tournois) waves dominate the dynamic characteristics of the interfacial crack propagation in PE–PM bi-material.

1. Introduction

Composites consisting of a PE phase and a PM phase are a class of newly emerging multifunctional materials which possess simultaneously PE, PM and magnetoelectric (ME) effects. Among these effects, the coupling between electrical and magnetic fields is a new product property that is absent in each constituent, and results from the mechanical interaction between PE and PM phases. The early investigations on the magnetoelectric effect of PE-PM composite materials (PPCMs) were carried out by van Suchtelen (1972), van den Boomgaard et al. (1974) and van den Boomgaard et al. (1976). Since then, especially in the past two decades, a great deal of work has been devoted to the prediction and determination of the ME effect in PPCMs with various microstructures both theoretically and experimentally. The comprehensive reviews of this research topic have been given by Nan et al. (2008) and Priya et al. (2007), respectively. Due to their ability of energy conversion between electric and magnetic fields, PPCMs are potential candidates for magnetic sensors, transducers and microwave devices, such as resonators, electric field tunable filters, phase shifters and delay lines.

With the rapid developments and potential applications of PPCMs (also called magneto-electro-elastic (MEE) materials in mechanics community), their fracture mechanics has attracted more and more attentions in recent years. This is because defects such as cracks, cavities, inclusions and dislocations may exist or arise in MEE materials during their manufacturing process or service and can greatly affect the reliability and integrity of MEE devices and structures. The static fracture problems of MEE materials have been extensively studied and can found in the literature. As Nan et al. (2008) have point out, MEE devices or structures are often subjected to dynamic mechanical and electromagnetic loads in operation. Therefore, it is worthwhile to analyze the dynamic fracture behaviors of MEE materials. To date, there were some investigations that took into account the dynamic fracture problems of the MEE materials. These studies include the transient response of the cracked solids under impact loads (Feng et al., 2005, 2009; Feng and Su, 2006, 2007; Feng and Liu, 2007; Li, 2005; Rangelov et al., 2011; Wang et al., 2010; Yong and Zhou, 2007; Zhong et al., 2009), the elastic wave scattering induced by cracks (Du et al., 2004; Feng et al., 2006; Li and Lee, 2009; Rojas et al., 2010; Zhang, 2011; Zhou and Wang, 2006, 2008) and the coupled fields produced by the moving crack at a constant speed and with a fixed length (Hu and Li, 2005; Hu et al., 2007; Zhong and Li, 2006; Tupholme, 2009).

Compared with the above-mentioned work, the exact analytical solutions for transient crack propagation in MEE materials are rather limited in the literature. Li and Mataga (1996) analyzed the transient response of a semi-infinite anti-plane crack propagating in a hexagonal PE medium with two kinds of boundary conditions: the conducting electrode type and a permeable vacuum free space, in

* Corresponding authors.
E-mail addresses: liujx02@hotmail.com (J.-x. Liu), fangdn@mail.tsinghua.edu.cn (D.-n. Fang).

0020-7683/$ - see front matter © 2012 Elsevier Ltd. All rights reserved.
http://dx.doi.org/10.1016/j.ijsolstr.2012.05.013

which the electrostatic potential is nonzero. Ing and Ma (1996, 1997) solved the problem of transient response of a finite crack subjected to dynamic anti-plane loading and an incident horizontally polarized shear wave. To et al. (2006) researched transient response of a mode-III interfacial crack propagating between two dissimilar piezoelectric half spaces and showed that the existence of the Maerfeld–Tournois (M–T) wave will increase the dynamic intensity factors and the dynamic free-energy release rate. Chen et al. (2008) studied the dynamic fracture problem of an elastic–piezoelectric bi-material containing a semi-infinite crack along the interface. The transient stress fields and the dynamic stress intensity factor are analyzed numerically. More recently, Chen (2009a) investigated the dynamic crack extension of anisotropic MEE solids and derived the dynamic energy release rate. Chen (2009b) further analyzed the propagation of a Mode III crack in a transversely isotropic MEE material. He numerically revealed the effects of magneto-electro-mechanical coupling coefficient and crack propagation velocity normalized dynamic stress intensity, normalized dynamic crack opening displacement intensity factor and normalized dynamic energy release rate.

In this paper, mode III interfacial crack propagating at a bi-material consisting of a PE half-space and PM half-space are researched. In Section 2, the constitutive equations and boundary conditions are described. In Sections 3 and 4, the Laplace transform technique in conjunction with the Wiener–Hopf and Cagniard–de Hoop techniques is employed to obtain the exact full-field solutions. To invest the crack tip field, in Section 5, the asymptotic solutions in the vicinity of the crack tip are given, and then the dynamic intensity factors of the stress, electric displacement and magnetic induction and the dynamic energy release rate are derived in explicit expressions. In Section 6, the numerical examples based on the analytical solutions are presented and discussed in detail.

2. Problem statement

Consider a semi-infinite crack along the interface between PE and PM half-spaces, as shown in Fig. 1. When time $t < 0$, the crack is assumed to be in a state of static equilibrium. At $t = 0^+$, a pair of concentrated longitudinal shear forces is applied on the surfaces of the crack, and the crack is assumed to propagate at a constant speed v. It was assumed the crack speed propagation is subsonic in order to maintain elliptic differential equations. All conclusions are therefore limited to subsonic crack propagation.

2.1. Governing equations

For the mode-III crack propagation problem, the anti-plane elastic deformation and the in-plane electromagnetic fields are coupled. Hence, the governing equations can be expressed as follows (Soh and Liu, 2006):

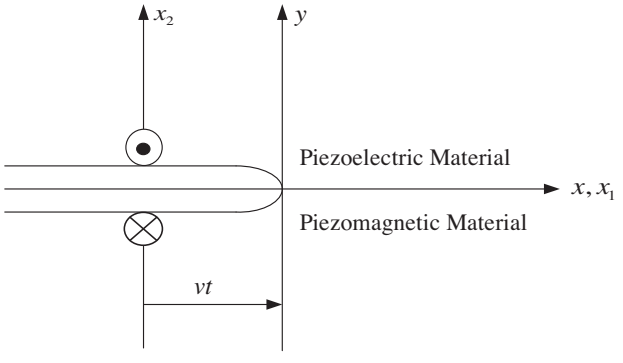

Fig. 1. A semi-infinite mode III interfacial propagating crack in a PE/PM bi-material.

$$\sigma_{3\beta}^e = c_{44}^e \frac{\partial u_3^e}{\partial x_\beta} + e_{15}\frac{\partial \phi^e}{\partial x_\beta}, \quad D_\beta^e = e_{15}\frac{\partial u_3^e}{\partial x_\beta} - \varepsilon_{11}^e \frac{\partial \phi^e}{\partial x_\beta}, \quad \beta = 1,2 \tag{1}$$

and

$$\sigma_{3\beta}^m = c_{44}^m \frac{\partial u_3^m}{\partial x_\beta} + h_{15}\frac{\partial \psi^m}{\partial x_\beta}, \quad B_\beta^m = h_{15}\frac{\partial u_3^m}{\partial x_\beta} - \mu_{11}^m \frac{\partial \psi^m}{\partial x_\beta}, \quad \beta = 1,2, \tag{2}$$

where the superscripts "e" and "m" denote the quantities in PE and PM media. u_3 and $\sigma_{3\beta}$ are the mechanical displacement and stress, ϕ and D_β are the electric potential and electric displacement, ψ and B_β are the magnetic potential and magnetic induction; C_{44}^e and C_{44}^m are the elastic constants in PE and PM media; e_{15} and h_{15} are PE and PM constants; ε_{11}^e and μ_{11}^m are the dielectric permittivity and magnetic permeability, respectively. The equations for functions with superscript "e" are in the domain $x_2 > 0$, while the equations for functions with superscripts "m" are in the domain $x_2 < 0$.

According to the usual quasi-static approximation, the equilibrium equations are

$$\frac{\partial \sigma_{31}^i}{\partial x_1} + \frac{\partial \sigma_{32}^i}{\partial x_2} = \rho^i \frac{\partial^2 u_3^i}{\partial t_2}, \quad \frac{\partial D_1^e}{\partial x_1} + \frac{\partial D_2^e}{\partial x_2} = 0, \quad \frac{\partial B_1^m}{\partial x_1} + \frac{\partial B_2^m}{\partial x_2} = 0 \quad (i = e,m), \tag{3}$$

where ρ^i is the mass density and t is the time.

Introduce a pseudo-electric Φ^e and a pseudo-magnetic potential functions Ψ^m

$$\Phi^e = \phi^e - \frac{e_{15}}{\varepsilon_{11}^e}u_3^e, \quad \Psi^m = \psi^m - \frac{h_{15}}{\mu_{11}^m}u_3^m. \tag{4}$$

We can derive the decoupled equations as follows:

$$c_{sh}^{e\,2}\nabla^2 u_3^e = \frac{\partial^2 u_3^e}{\partial t^2}, \quad \nabla^2 \Phi^e = 0 \tag{5}$$

and

$$c_{sh}^{m\,2}\nabla^2 u_3^m = \frac{\partial^2 u_3^m}{\partial t^2}, \nabla^2 \Psi^m = 0. \tag{6}$$

where $c_{sh}^e = \sqrt{\bar{c}_{44}^e/\rho^e}$ and $c_{sh}^m = \sqrt{\bar{c}_{44}^m/\rho^m}$ are the velocities of the bulk shear waves in a PE medium and a PM medium, $\bar{c}_{44}^e = c_{44}^e + e_{15}^2/\varepsilon_{11}^e$ and $\bar{c}_{44}^m = c_{44}^m + h_{15}^2/\mu_{11}^m$ are constants with the PE and PM effects, $\nabla^2 = \partial^2/\partial x_1^2 + \partial^2/\partial x_2^2$ is the two-dimensional Laplacian operator.

For crack propagation problems with a constant velocity (Freund, 1990), it is usually convenient to introduce a moving coordinate system:

$$x = x_1 - vt, y = x_2, z = x_3. \tag{7}$$

By making use of Eq. (7), the governing equations in the moving coordinate system can be changed into:

$$\begin{aligned} &\lambda_e^2 \frac{\partial^2 u_3^e}{\partial x^2} + \frac{\partial^2 u_3^e}{\partial y^2} + \frac{2v}{c_{sh}^{e2}}\frac{\partial^2 u_3^e}{\partial x \partial t} - \frac{1}{c_{sh}^{e2}}\frac{\partial^2 u_3^e}{\partial t^2} = 0, \\ &\frac{\partial^2 \Phi^e}{\partial x^2} + \frac{\partial^2 \Phi^e}{\partial y^2} = 0, \end{aligned} \tag{8}$$

$$\begin{aligned} &\lambda_m^2 \frac{\partial^2 u_3^m}{\partial x^2} + \frac{\partial^2 u_3^m}{\partial y^2} + \frac{2v}{c_{sh}^{m2}}\frac{\partial^2 u_3^m}{\partial x \partial t} - \frac{1}{c_{sh}^{m2}}\frac{\partial^2 u_3^m}{\partial t^2} = 0, \\ &\frac{\partial^2 \Phi^m}{\partial x^2} + \frac{\partial^2 \Phi^m}{\partial y^2} = 0, \end{aligned} \tag{9}$$

where $\lambda_i = \sqrt{1 - (v/c_{sh}^i)^2}, i = e,m.$

2.2. Boundary conditions

As is customary in linear transient crack growth problems (Freund, 1972), the remote boundary conditions maybe taken as:

$$\begin{cases} u_3^e(x,y,t)=0, & \Phi^e(x,y,t)=0, \quad y\to+\infty, \\ u_3^m(x,y,t)=0, & \Psi^m(x,y,t)=0, \quad y\to-\infty. \end{cases} \tag{10}$$

Here, the fundamental solution of transient crack propagation under a pair of concentrated loads acting on the crack surface is considered and the corresponding mechanical boundary conditions are imposed

$$\sigma_{3y}^e(x,0,t)=\sigma_{3y}^m(x,0,t)=-\delta(x)H(t), \quad x<vt, \tag{11}$$

$$u_3^e=u_3^m, \quad x>vt. \tag{12}$$

where δ is the Dirac delta function and $H(t)$ is the Heaviside function.

For PE/PM composite materials, the conversion of energy between electric and magnetic fields is depended on the electro-elastic fields in PE phase and the magnetoelastic fields in PM phase (Bichurin et al., 2003; Nan et al., 2008; Priya et al., 2007). This means that the magnetic field in PE phase and the electric field in can be neglected. Therefore, the electric and magnetic potentials on the interface and crack faces can be taken as zero, i.e.

$$\begin{cases} \phi^e(x,0,t)=0, & -\infty<x<+\infty, \\ \psi^m(x,0,t)=0, & -\infty<x<+\infty. \end{cases} \tag{13}$$

The above conditions have been adopted by Melkumyan and Mai (2008) and Huang et al. (2009) for SH waves propagating in PE–PM bi-materials, respectively.

The quiescent initial conditions are

$$\begin{cases} u_3^e(x,y,0)=u_3^m(x,y,0)=0, & \dot{u}_3^e(x,y,0)=\dot{u}_3^m(x,y,0)=0 \\ \phi^e(x,y,0)=0, & \dot{\phi}^e(x,y,0)=0 \\ \psi^m(x,y,0)=0, & \dot{\psi}^m(x,y,0)=0 \end{cases} \tag{14}$$

where the dot over variable denotes material time derivative.

3. Solutions in the transformed domain

3.1. Laplace transform

The mixed initial boundary problem in the previous section will be solved by using the standard procedure of Laplace transforms. To suppress the time variable t, the one-sided Laplace transform is applied:

$$f^*(x,y,p)=\int_0^\infty f(x,y,t)\exp(-pt)dt, \tag{15}$$

$$f(x,y,t)=\frac{1}{2\pi i}\int_{B_{r1}} f^*(x,y,p)\exp(pt)dp, \tag{16}$$

To suppress the spatial variable x, the two-sided Laplace transform is imposed:

$$\hat{f}^*(\xi,y,p)=\int_{-\infty}^{\infty} f^*(x,y,p)\exp(-p\xi x)dx, \tag{17}$$

$$f^*(x,y,p)=\frac{p}{2\pi i}\int_{B_{r2}} \hat{f}^*(\xi,y,p)\exp(p\xi x)d\xi, \tag{18}$$

where the inversion integration is surrounded by the usual Bromwich path.

Applying the transformations, the governing equations (8) and (9) become:

$$\left.\begin{aligned} &\left[\tfrac{d^2}{dy^2}-p^2\left(\tfrac{1}{c_{sh}^{e2}}-2\tfrac{v}{c_{sh}^{e2}}\xi-\lambda^{e2}\xi^2\right)\right]\hat{u}_3^{e*}(\xi,y,p)=0, \\ &\left[\tfrac{d^2}{dy^2}-p^2(\varepsilon^2-\xi^2)\right]\hat{\Phi}^{e*}(\xi,y,p)=0, \end{aligned}\right\} y>0, \tag{19}$$

$$\left.\begin{aligned} &\left[\tfrac{d^2}{dy^2}-p^2\left(\tfrac{1}{c_{sh}^{m2}}-2\tfrac{v}{c_{sh}^{m2}}\xi-\lambda^{m2}\xi^2\right)\right]\hat{u}_3^{m*}(\xi,y,p)=0, \\ &\left[\tfrac{d^2}{dy^2}-p^2(\varepsilon^2-\xi^2)\right]\hat{\Psi}^{m*}(\xi,y,p)=0, \end{aligned}\right\} y<0. \tag{20}$$

Considering the boundary conditions at infinity, and the solutions to Eqs. (19) and (20) can be chosen as:

$$\left.\begin{aligned} \hat{u}_3^{e*}(\xi,y,p)&=\tfrac{1}{p^2}A^e(\xi)\exp(-p\alpha^e y) \\ \hat{\Phi}^{e*}(\xi,y,p)&=\tfrac{1}{p^2}B^e(\xi)\exp(-p\beta^e y) \end{aligned}\right\} y>0, \tag{21}$$

$$\left.\begin{aligned} \hat{u}_3^{m*}(\xi,y,p)&=-\tfrac{1}{p^2}A^m(\xi)\exp(p\alpha^m y) \\ \hat{\Psi}^{m*}(\xi,y,p)&=-\tfrac{1}{p^2}B^m(\xi)\exp(p\beta^m y) \end{aligned}\right\} y<0, \tag{22}$$

where the coefficient functions $\alpha^e(\xi)$, $\alpha^m(\xi)$ and $\beta(\xi)$ are

$$\alpha^e(\xi)\triangleq\sqrt{\frac{1}{c_{sh}^{e2}}-2\frac{v}{c_{sh}^{e2}}\xi-\lambda_e^2\xi^2}=\lambda_e\sqrt{\left(\xi+\frac{1}{c_{sh}^e-v}\right)\left(\frac{1}{c_{sh}^e+v}-\xi\right)}, \tag{23}$$

$$\alpha^m(\xi)\triangleq\sqrt{\frac{1}{c_{sh}^{m2}}-2\frac{v}{c_{sh}^{m2}}\xi-\lambda_m^2\xi^2}=\lambda_m\sqrt{\left(\xi+\frac{1}{c_{sh}^m-v}\right)\left(\frac{1}{c_{sh}^m+v}-\xi\right)}, \tag{24}$$

$$\beta^e(\xi)=\beta^m(\xi)=\beta(\xi)\triangleq\lim_{\varepsilon\to0}\sqrt{\varepsilon^2-\xi^2}. \tag{25}$$

Here ε is introduced as an auxiliary perturbation parameter (Li and Mataga, 1996), with the understanding that whenever ε is present, the final expressions involved are always evaluated at $\varepsilon=0$ at the end of the manipulation.

Substitution of solutions (21) and (22) into the transformed continuity condition equation (13) leads to

$$B^e(\xi)=-\frac{e_{15}}{\varepsilon_{11}^e}A^e(\xi), \tag{26}$$

$$B^m(\xi)=-\frac{h_{15}}{\mu_{11}^m}A^m(\xi). \tag{27}$$

Inserting Eqs. (26) and (27) into the solutions in Eqs. (21) and (22) and then making use of the inverse transform (18), one gets

$$\begin{aligned} u_3^{e*}(x,y,p)&=\frac{1}{2\pi ip}\int_{\xi_\alpha^e-i\infty}^{\xi_\alpha^e+i\infty}A^e(\xi)\exp(-p(\alpha^e(\xi)y-\xi x))d\xi, \\ \Phi^{e*}(x,y,p)&=-\frac{e_{15}}{2\pi ip\varepsilon_{11}^e}\int_{\xi_\beta^e-i\infty}^{\xi_\beta^e+i\infty}A^e(\xi)\exp(-p(\beta^e(\xi)y-\xi x))d\xi, \end{aligned} \tag{28}$$

$$\begin{aligned} u_3^{m*}(x,y,p)&=-\frac{1}{2\pi ip}\int_{\xi_\alpha^m-i\infty}^{\xi_\alpha^m+i\infty}A^m(\xi)\exp(p(\alpha^m(\xi)y+\xi x))d\xi, \\ \Psi^{m*}(x,y,p)&=\frac{h_{15}}{2\pi ip\mu_{11}^m}\int_{\xi_\beta^m-i\infty}^{\xi_\beta^m+i\infty}A^m(\xi)\exp(p(\beta^m(\xi)y+\xi x))d\xi. \end{aligned} \tag{29}$$

3.2. Expanding the boundary conditions

Next task is to seek the solutions that satisfy the conditions (11) and (12) in the transformed space by employing the Wiener–Hopf decomposition method. It is necessary to expand the displacement and stress boundary conditions over the full range of the x-axis. So we introduce the following two unknown functions:

$$\Delta u_{3-}(x,t)=\begin{cases} 0, & x\leqslant 0, \\ u_3^e(x,0,t)-u_3^m(x,0,t), & x\leqslant 0, \end{cases} \tag{30}$$

$$\sigma_+(x,t)=\begin{cases}\sigma^e_{yz}(x,0,t)=\sigma^m_{yz}(x,0,t), & x\leqslant 0,\\ 0, & x\leqslant 0.\end{cases} \tag{31}$$

Such that:

$$u^e_3(x,0,t)-u^m_3(x,0,t)=\Delta u_{3-}(x,t),\quad -\infty<x<\infty, \tag{32}$$

$$\sigma^e_{yz}(x,0,t)=\sigma^m_{yz}(x,0,t)=\sigma_+(x,t)-\delta(x+vt)H(t),\quad -\infty<x<\infty. \tag{33}$$

After suppressing both x and t:

$$\hat{u}^{e*}_3(\xi,0,p)-\hat{u}^{m*}_3(\xi,0,p)=\frac{\Delta W_-(\xi)}{p^2}, \tag{34}$$

$$\hat{\sigma}^{e*}_{yz}(\xi,0,p)=\hat{\sigma}^{m*}_{yz}(\xi,0,p)=\frac{\Sigma_+(\xi)}{p}+\frac{1}{pv}\frac{1}{(\xi-1/v)}, \tag{35}$$

where

$$\Delta W_-(\xi)=p^2\int_{-\infty}^{0}\Delta u^*_{3-}(x,p)\exp(-p\xi x)dx, \tag{36}$$

$$\Sigma_+(\xi)=p\int_0^{\infty}\sigma^*_+(x,p)\exp(-p\xi x)dx. \tag{37}$$

At the same time, substituting the solutions Eqs. (21) and (22) with Eqs. (26) and (27) into the transformed constitutive equations, one finds that

$$A^e(\xi)=-\frac{p}{B^e_G(\xi)}\hat{\sigma}^{e*}_{yz}(\xi,0,p),\quad A^m(\xi)=-\frac{p}{B^m_G(\xi)}\hat{\sigma}^{m*}_{yz}(\xi,0,p), \tag{38}$$

where

$$B^e_G(\xi)=\bar{c}^e_{44}[\alpha^e(\xi)-k^2_e\beta(\xi)],\quad B^m_G(\xi)=\bar{c}^m_{44}[\alpha^m(\xi)-k^2_m\beta(\xi)] \tag{39}$$

can be considered as the B–G wave functions for the PE and PM half spaces, respectively. k^2_e and k^2_m are

$$k^2_e=e^2_{15}/(\bar{c}^e_{44}\varepsilon^e_{11}),\quad k^2_m=h^2_{15}/(\bar{c}^m_{44}\mu^m_{11}), \tag{40}$$

where k^2_e is the electro-mechanical coupling coefficient in a PE material and k^2_m the magneto-mechanical coupling coefficient in a PM material.

3.3. The Wiener–Hopf solution

Substituting Eqs. (21) and (22) with Eq. (38) into Eq. (34), we can obtain the standard Wiener–Hopf equation

$$\Sigma_+(\xi)+\frac{1}{v(\xi-1/v)}=K(\xi)\Delta W_-(\xi) \tag{41}$$

where $K(\xi)=-B^e_G(\xi)B^m_G(\xi)/M_T(\xi)$, $M_T(\xi)=B^e_G(\xi)+B^m_G(\xi)$. $M_T(\xi)$ can be considered as the generalized M–T wave function.

The key to solving Eq. (41) is to factorize $K(\xi)$ into sectionally analytical functions in the left and right half complex planes. Here define the B–G wave speeds for PE and PM half spaces as follows:

$$c^e_{bg}=c^e_{sh}\sqrt{1-k^4_e},\quad c^m_{bg}=c^m_{sh}\sqrt{1-k^4_m}. \tag{42}$$

Following the arguments (Li and Mataga, 1996; To et al., 2006), $B^e_G(\xi)$ and $B^m_G(\xi)$ can be decomposed into the following forms

$$B^e_G(\xi)=\frac{(1/(c^e_{bg}-v)+\xi)(1/(c^e_{bg}+v)-\xi)}{\sqrt{(1/(c^e_{sh}-v)+\xi)(1/(c^e_{sh}+v)-\xi)}}T^e_+(\xi)T^e_-(\xi)B^e_{Gs}(v), \tag{43}$$

$$B^m_G(\xi)=\frac{(1/(c^m_{bg}-v)+\xi)(1/(c^m_{bg}+v)-\xi)}{\sqrt{(1/(c^m_{sh}-v)+\xi)(1/(c^m_{sh}+v)-\xi)}}T^m_+(\xi)T^m_-(\xi)B^m_{Gs}(v), \tag{44}$$

where

$$\begin{cases}B^i_{GS}(v)=\bar{c}^i_{44}(\lambda_i-k^2_i),\\ T^i_{\pm}(\xi)=\exp\left\{-\frac{1}{\pi}\int_{\varepsilon}^{1/(c^i_{sh}\mp v)}\tan^{-1}(E^i(\mp\eta))\frac{d\eta}{\eta\pm\xi}\right\}, & i=e,m\\ E^i(\eta)=\frac{k^2_i\eta}{\lambda_i\sqrt{(1/(c^i_{sh}-v)+\eta)(1/(c^i_{sh}+v)-\eta)}}.\end{cases} \tag{45}$$

If the generalized M–T wave exists, there is a real root ξ to satisfy the generalized M–T wave equation

$$M_T(\xi)=\bar{c}^e_{44}\alpha^e(\xi)+\bar{c}^m_{44}\alpha^m(\xi)-(\bar{c}^e_{44}k^2_e+\bar{c}^m_{44}k^2_m)\beta(\xi)=0 \tag{46}$$

When $k_m=0$, Eq. (46) can retard to the problem of dynamic interfacial crack propagation in elastic–piezoelectric bi-materials (Chen et al., 2008).

Chen et al. (2008) also gave the discussion about the existence of a real root in detail. Here, we follow the same procedure, and some results are used. They are listed in Table 1.

Furthermore, we call the real root ξ which satisfies Eq. (46) the generalized M–T wave speed. If the generalized M–T wave does not exist, there is no M–T wave. When Eq. (46) has two distinct real roots, $-\frac{1}{c_{mt}-v}$ and $\frac{1}{c_{mt}+v}$.

In which

$$c_{mt}=\sqrt{2A_1/(-B_1-\sqrt{B^2_1-4A_1C_1})}$$

$$A_1=[1+(\bar{c}^e_{44}/\bar{c}^m_{44})^2-(k^2_m+k^2_e\bar{c}^e_{44}/\bar{c}^m_{44})^2]^2-4(\bar{c}^e_{44}/\bar{c}^m_{44})^2,$$

$$B_1=-2[1/c^{e2}_{sh}+(\bar{c}^e_{44}/\bar{c}^m_{44})^2/c^{m2}_{sh}][1+(\bar{c}^e_{44}/\bar{c}^m_{44})^2-(k^2_m+k^2_e\bar{c}^e_{44}/\bar{c}^m_{44})^2]+4(\bar{c}^e_{44}/\bar{c}^m_{44})^2(1/c^{e2}_{sh}+1/c^{m2}_{sh}),$$

$$C_1=1/c^{e4}_{sh}-2(\bar{c}^e_{44}/\bar{c}^m_{44})^2/c^{e2}_{sh}/c^{m2}_{sh}+(\bar{c}^e_{44}/\bar{c}^m_{44})^4/c^{m4}_{sh}.$$

Four cases for the existence of generalized M-T wave will be discussed as follows:

Case (1): $c^e_{sh}\geqslant c^m_{sh}$ (The existence of generalized MT wave)

We introduce a new function $S^*_1(\xi)$ as follows:

$$S^*_1(\xi)=\frac{M_T(\xi)}{\sqrt{\frac{1}{c_{mt}-v}+\xi}\sqrt{\frac{1}{c_{mt}+v}-\xi}}\frac{1}{B^e_{GS}(v)+B^m_{GS}(v)}. \tag{47}$$

The function $S^*_1(\xi)$ has the property that $S^*_1(\xi)\to 1$ as $|\xi|\to\infty$, and $S^*_1(\xi)$ has neither poles nor zeros in the ξ-plane by cuts along $-\frac{1}{c_{mt}-v}<\xi<-\varepsilon$ and $\varepsilon<\xi<\frac{1}{c_{mt}+v}$. By using the general product factorization method, $S^*_1(\xi)$ can be further decomposed as the product of two regular functions $S^*_{1+}(\xi)$ and $S^*_{1-}(\xi)$, where

$$S^*_{1\pm}(\xi)=\frac{\sqrt{\frac{1}{c_{mt}\mp v}\pm\xi}}{\sqrt{\frac{1}{c^m_{sh}\mp v}\pm\xi}}Q^*_{1\pm}(\xi) \tag{48}$$

in which

Table 1
Existence condition for the real roots.

Case	Condition	Existence
$c^e_{sh}<c^m_{sh}$	$\mathrm{Im}[M_T(1/(c^e_{sh}+v))]>0$ and $\mathrm{Im}[M_T(1/(v-c^e_{sh}))]>0$	No
	$\mathrm{Im}[M_T(1/(c^e_{sh}+v))]<0$ and $\mathrm{Im}[M_T(1/(v-c^e_{sh}))]<0$	Yes
$c^e_{sh}>c^m_{sh}$	$\mathrm{Im}[M_T(1/(c^m_{sh}+v))]>0$ and $\mathrm{Im}[M_T(1/(v-c^m_{sh}))]>0$	No
	$\mathrm{Im}[M_T(1/(c^m_{sh}+v))]<0$ and $\mathrm{Im}[M_T(1/(v-c^m_{sh}))]<0$	Yes

$$Q^*_{1\pm}(\xi)=\exp\left\{-\frac{1}{\pi}\int_{\varepsilon}^{\frac{1}{c^m_{sh}\mp v}}\tan^{-1}\left[\frac{\Im(M_T(\mp\eta))}{\Re(M_T(\mp\eta))}\right]\frac{d\eta}{\eta\pm\xi}\right\}$$
$$=\exp\left\{-\frac{1}{\pi}\int_{\frac{1}{c^e_{sh}\mp v}}^{\frac{1}{c^m_{sh}\mp v}}\tan^{-1}\left[\frac{(\bar c^e_{44}k_e^2+\bar c^m_{44}k_m^2)\eta-\bar c^e_{44}\sqrt{\lambda_e^2\eta^2\mp\frac{2v\eta}{c^{e2}_{sh}}-\frac{1}{c^{e2}_{sh}}}}{\bar c^m_{44}\alpha^m(\mp\eta)}\right]\frac{d\eta}{\eta\pm\xi}\right\}$$
$$\times\exp\left\{-\frac{1}{\pi}\int_{\varepsilon}^{\frac{1}{c^e_{sh}\mp v}}\tan^{-1}\left[\frac{(\bar c^e_{44}k_e^2+\bar c^m_{44}k_m^2)\eta}{\bar c^m_{44}\alpha^m(\mp\eta)+\bar c^e_{44}\alpha^e(\mp\eta)}\right]\frac{d\eta}{\eta\pm\xi}\right\},\tag{49}$$

in which $\Im(M_T(\eta))$ and $\Re(M_T(\eta))$ denote the imaginary part and real part of $M_T(\eta)$, respectively.

Then

$$M_T(\xi)=\frac{\left(\frac{1}{c_{mt}-v}+\xi\right)\left(\frac{1}{c_{mt}+v}-\xi\right)}{\sqrt{\frac{1}{c^m_{sh}-v}+\xi}\sqrt{\frac{1}{c^m_{sh}+v}-\xi}}Q^*_{1+}(\xi)Q^*_{1-}(\xi)(B^e_{GS}(v)+B^m_{GS}(v)).\tag{50}$$

Case (2): $c^e_{sh}\geqslant c^m_{sh}$ (No generalized M–T surface wave)

We introduced a new function $Q^*_2(\xi)$ as

$$Q^*_2(\xi)=\frac{M_T(\xi)}{\sqrt{\frac{1}{c^m_{sh}-v}+\xi}\sqrt{\frac{1}{c^m_{sh}+v}-\xi}}\frac{1}{B^e_{GS}(v)+B^m_{GS}(v)}.\tag{51}$$

The function $Q^*_2(\xi)$ has the property that $Q^*_2(\xi)\to 1$ as $|\xi|\to\infty$, and $Q^*_2(\xi)$ has neither poles nor zeros in the ξ-plane by cuts along $-\frac{1}{c^m_{sh}-v}<\xi<-\varepsilon$ and $\varepsilon<\xi<\frac{1}{c^m_{sh}+v}$. By using the general product factorization method, $Q^*_2(\xi)$ can be further decomposed as the product of two regular functions $Q^*_{2+}(\xi)$ and $Q^*_{2-}(\xi)$, where

$$Q^*_{2\pm}(\xi)=\exp\left\{-\frac{1}{\pi}\int_{\varepsilon}^{\frac{1}{c^m_{sh}\mp v}}\tan^{-1}\left[\frac{\Im(M_T(\mp\eta))}{\Re(M_T(\mp\eta))}\right]\frac{d\eta}{\eta\pm\xi}\right\}$$
$$=\exp\left\{-\frac{1}{\pi}\int_{\frac{1}{c^e_{sh}\mp v}}^{\frac{1}{c^m_{sh}\mp v}}\tan^{-1}\left[\frac{(\bar c^e_{44}k_e^2+\bar c^m_{44}k_m^2)\eta-\bar c^e_{44}\sqrt{\lambda_e^2\eta^2\mp\frac{2v\eta}{c^{e2}_{sh}}-\frac{1}{c^{e2}_{sh}}}}{\bar c^m_{44}\alpha^m(\mp\eta)}\right]\frac{d\eta}{\eta\pm\xi}\right\}$$
$$\times\exp\left\{-\frac{1}{\pi}\int_{\varepsilon}^{\frac{1}{c^e_{sh}\mp v}}\tan^{-1}\left[\frac{(\bar c^e_{44}k_e^2+\bar c^m_{44}k_m^2)\eta}{\bar c^m_{44}\alpha^m(\mp\eta)+\bar c^e_{44}\alpha^e(\mp\eta)}\right]\frac{d\eta}{\eta\pm\xi}\right\}=Q^*_{1\pm}(\xi).\tag{52}$$

Then

$$M_T(\xi)=\sqrt{\frac{1}{c^m_{sh}-v}+\xi}\sqrt{\frac{1}{c^m_{sh}+v}-\xi}Q^*_{1+}(\xi)Q^*_{1-}(\xi)(B^e_{GS}(v)+B^m_{GS}(v))$$
$$=\frac{\left(\frac{1}{c^m_{sh}-v}+\xi\right)\left(\frac{1}{c^m_{sh}+v}-\xi\right)}{\sqrt{\frac{1}{c^m_{sh}-v}+\xi}\sqrt{\frac{1}{c^m_{sh}+v}-\xi}}Q^*_{1+}(\xi)Q^*_{1-}(\xi)(B^e_{GS}(v)+B^m_{GS}(v)).\tag{53}$$

Compared with Eqs. (50), $M_T(\xi)$ for cases (1) and (2) can be written in a unified form, where

$$M_T(\xi)=\frac{\left(\frac{1}{c-v}+\xi\right)\left(\frac{1}{c+v}-\xi\right)}{\sqrt{\frac{1}{c^m_{sh}-v}+\xi}\sqrt{\frac{1}{c^m_{sh}+v}-\xi}}Q^*_{1+}(\xi)Q^*_{1-}(\xi)(B^e_{GS}(v)+B^m_{GS}(v))\tag{54}$$

in which

$$c\triangleq\begin{cases}c_{mt} & \text{if the generalized MT wave exists,}\\ c^m_{sh} & \text{otherwise.}\end{cases}\tag{55}$$

Case (3): $c^e_{sh}\leqslant c^m_{sh}$ (The existence of generalized M–T wave)

We introduce a new function $S^*_3(\xi)$ as follows:

$$S^*_3(\xi)=\frac{M_T(\xi)}{\sqrt{\frac{1}{c_{mt}-v}+\xi}\sqrt{\frac{1}{c_{mt}+v}-\xi}}\frac{1}{B^e_{GS}(v)+B^m_{GS}(v)}\tag{56}$$

The function $S^*_3(\xi)$ has the property that $S^*_3(\xi)\to 1$ as $|\xi|\to\infty$, and $S^*_3(\xi)$ has neither poles nor zeros in the ξ-plane by cuts along $-\frac{1}{c_{mt}-v}<\xi<-\varepsilon$ and $\varepsilon<\xi<\frac{1}{c_{mt}+v}$. By using the general product factorization method, $S^*_3(\xi)$ can be further decomposed as the product of two regular functions $S^*_{3+}(\xi)$ and $S^*_{3-}(\xi)$, where

$$S^*_{3\pm}(\xi)=\frac{\sqrt{\frac{1}{c_{mt}\mp v}\pm\xi}}{\sqrt{\frac{1}{c^e_{sh}\mp v}\pm\xi}}Q^*_{3\pm}(\xi)\tag{57}$$

in which

$$Q^*_{3\pm}(\xi)=\exp\left\{-\frac{1}{\pi}\int_{\varepsilon}^{\frac{1}{c^e_{sh}\mp v}}\tan^{-1}\left[\frac{\Im(M_T(\mp\eta))}{\Re(M_T(\mp\eta))}\right]\frac{d\eta}{\eta\pm\xi}\right\}$$
$$=\exp\left\{-\frac{1}{\pi}\int_{\frac{1}{c^m_{sh}\mp v}}^{\frac{1}{c^e_{sh}\mp v}}\tan^{-1}\left[\frac{(\bar c^e_{44}k_e^2+\bar c^m_{44}k_m^2)\eta-\bar c^m_{44}\sqrt{\lambda_m^2\eta^2\mp\frac{2v\eta}{c^{m2}_{sh}}-\frac{1}{c^{m2}_{sh}}}}{\bar c^e_{44}\alpha^e(\mp\eta)}\right]\frac{d\eta}{\eta\pm\xi}\right\}$$
$$\times\exp\left\{-\frac{1}{\pi}\int_{\varepsilon}^{\frac{1}{c^m_{sh}\mp v}}\tan^{-1}\left[\frac{(\bar c^e_{44}k_e^2+\bar c^m_{44}k_m^2)\eta}{\bar c^m_{44}\alpha^m(\mp\eta)+\bar c^e_{44}\alpha^e(\mp\eta)}\right]\frac{d\eta}{\eta\pm\xi}\right\}\tag{58}$$

Then

$$M_T(\xi)=\frac{\left(\frac{1}{c_{mt}-v}+\xi\right)\left(\frac{1}{c_{mt}+v}-\xi\right)}{\sqrt{\frac{1}{c^e_{sh}-v}+\xi}\sqrt{\frac{1}{c^e_{sh}+v}-\xi}}Q^*_{3+}(\xi)Q^*_{3-}(\xi)(B^e_{GS}(v)+B^m_{GS}(v)).\tag{59}$$

Case (4): $c^e_{sh}\leqslant c^m_{sh}$ (No generalized M–T surface wave)

We introduced a new function $Q^*_4(\xi)$ as

$$Q^*_4(\xi)=\frac{M_T(\xi)}{\sqrt{\frac{1}{c^e_{sh}-v}+\xi}\sqrt{\frac{1}{c^e_{sh}+v}-\xi}}\frac{1}{B^e_{GS}(v)+B^m_{GS}(v)}\tag{60}$$

The function $Q^*_4(\xi)$ has the property that $Q^*_4(\xi)\to 1$ as $|\xi|\to\infty$, and $Q^*_4(\xi)$ has neither poles nor zeros in the ξ -plane by cuts along $-\frac{1}{c^e_{sh}-v}<\xi<-\varepsilon$ and $\varepsilon<\xi<\frac{1}{c^e_{sh}+v}$. By using the general product factorization method, $Q^*_4(\xi)$ can be further decomposed as the product of two regular functions $Q^*_{4+}(\xi)$ and $Q^*_{4-}(\xi)$, where

$$Q^*_{4\pm}(\xi)=\exp\left\{-\frac{1}{\pi}\int_{\varepsilon}^{\frac{1}{c^e_{sh}\mp v}}\tan^{-1}\left[\frac{\Im(M_T(\mp\eta))}{\Re(M_T(\mp\eta))}\right]\frac{d\eta}{\eta\pm\xi}\right\}$$
$$=\exp\left\{-\frac{1}{\pi}\int_{\frac{1}{c^m_{sh}\mp v}}^{\frac{1}{c^e_{sh}\mp v}}\tan^{-1}\left[\frac{(\bar c^e_{44}k_e^2+\bar c^m_{44}k_m^2)\eta-\bar c^m_{44}\sqrt{\lambda_m^2\eta^2\mp\frac{2v\eta}{c^{m2}_{sh}}-\frac{1}{c^{m2}_{sh}}}}{\bar c^e_{44}\alpha^e(\mp\eta)}\right]\frac{d\eta}{\eta\pm\xi}\right\}$$
$$\times\exp\left\{-\frac{1}{\pi}\int_{\varepsilon}^{\frac{1}{c^m_{sh}\mp v}}\tan^{-1}\left[\frac{(\bar c^e_{44}k_e^2+\bar c^m_{44}k_m^2)\eta}{\bar c^m_{44}\alpha^m(\mp\eta)+\bar c^e_{44}\alpha^e(\mp\eta)}\right]\frac{d\eta}{\eta\pm\xi}\right\}=Q^*_{3\pm}(\xi).\tag{61}$$

Then

$$M_T(\xi)=\sqrt{\frac{1}{c^e_{sh}-v}+\xi}\sqrt{\frac{1}{c^e_{sh}+v}-\xi}Q^*_{3+}(\xi)Q^*_{3-}(\xi)(B^e_{GS}(v)+B^m_{GS}(v))$$
$$=\frac{\left(\frac{1}{c^e_{sh}-v}+\xi\right)\left(\frac{1}{c^e_{sh}+v}-\xi\right)}{\sqrt{\frac{1}{c^e_{sh}-v}+\xi}\sqrt{\frac{1}{c^e_{sh}+v}-\xi}}Q^*_{3+}(\xi)Q^*_{3-}(\xi)(B^e_{GS}(v)+B^m_{GS}(v))\tag{62}$$

Compared with Eq. (59), $M_T(\xi)$ for cases (3) and (4) can be written in a unified form, where:

$$M_T(\xi)=\frac{\left(\frac{1}{c-v}+\xi\right)\left(\frac{1}{c+v}-\xi\right)}{\sqrt{\frac{1}{c^e_{sh}-v}+\xi}\sqrt{\frac{1}{c^e_{sh}+v}-\xi}}Q^*_{3+}(\xi)Q^*_{3-}(\xi)(B^e_{GS}(v)+B^m_{GS}(v))\tag{63}$$

in which

$$c\triangleq\begin{cases}c_{mt} & \text{if the generalized MT wave exists,}\\ c^e_{sh} & \text{otherwise.}\end{cases}\tag{64}$$

To solve the Wiener–Hopf equation (41), we introduce the following expression:

$$Q(v)=\frac{B^e_{Gs}(v)B^m_{Gs}(v)}{B^e_{Gs}(v)+B^m_{Gs}(v)},\quad F_+(\xi)=\frac{T^e_+(\xi)T^m_+(\xi)}{S_+(\xi)},$$
$$F_-(\xi)=\frac{T^e_-(\xi)T^m_-(\xi)}{S_-(\xi)}, \tag{65}$$

$$G_+(\xi)=\frac{1}{F_+(\xi)}\frac{(1/(c-v)+\xi)\sqrt{(1/(c^e_{sh}-v)+\xi)}}{(1/(c^e_{bg}-v)+\xi)(1/(c^m_{bg}-v)+\xi)},$$
$$G_-(\xi)=\frac{1}{F_-(\xi)}\frac{(1/(c+v)-\xi)\sqrt{(1/(c^e_{sh}+v)-\xi)}}{(1/(c^e_{bg}+v)-\xi)(1/(c^m_{bg}+v)-\xi)}. \tag{66}$$

By using the procedure presented by in Noble (1958), the solution to the Wiener–Hopf equation (41) can be found

$$\Delta W_-(\xi)=-\frac{G_-(\xi)}{v(\xi-1/v)}\frac{G_+(1/v)}{Q(v)}. \tag{67}$$

$$\Sigma_+(\xi)=\frac{1}{v(\xi-1/v)}\left(\frac{G_+(1/v)}{G_+(\xi)}-1\right). \tag{68}$$

The functions $A^e(\xi)$ and $A^m(\xi)$ can be determined as

$$\begin{aligned}A^e(\xi)&=-\frac{G_+(1/v)}{\bar{c}^e_{44}(\alpha^e(\xi)-k_e^2\beta(\xi))v(\xi-1/v)G_+(\xi)}\\&=-\frac{c(c^e_{bg}-v)(c^m_{bg}-v)}{\bar{c}^e_{44}(\alpha^e(\xi)-k_e^2\beta(\xi))v(\xi-1/v)c^e_{bg}c^m_{bg}(c-v)}\\&\times\frac{(1/(c^e_{bg}-v)+\xi)(1/(c^m_{bg}-v)+\xi)}{(1/(c-v)+\xi)\sqrt{(1/(c^e_{sh}-v)+\xi)}}\sqrt{\frac{vc^e_{sh}}{(c^e_{sh}-v)}}\frac{F_+(\xi)}{F_+(1/v)},\end{aligned} \tag{69}$$

$$\begin{aligned}A^m(\xi)&=-\frac{G_+(1/v)}{\bar{c}^m_{44}(\alpha^m(\xi)-k_m^2\beta(\xi))v(\xi-1/v)G_+(\xi)}\\&=-\frac{c(c^e_{bg}-v)(c^m_{bg}-v)}{\bar{c}^m_{44}(\alpha^m(\xi)-k_m^2\beta(\xi))v(\xi-1/v)c^e_{bg}c^m_{bg}(c-v)}\\&\times\frac{(1/(c^e_{bg}-v)+\xi)(1/(c^m_{bg}-v)+\xi)}{(1/(c-v)+\xi)\sqrt{(1/(c^e_{sh}-v)+\xi)}}\sqrt{\frac{vc^e_{sh}}{(c^e_{sh}-v)}}\frac{F_+(\xi)}{F_+(1/v)}.\end{aligned} \tag{70}$$

With $A^e(\xi)$ and $A^m(\xi)$ in hand, the function $B^i(\xi)$ can be determined from Eqs. (26) and (27).

4. Solutions in the physical domain

In this section, we shall derive the explicit solutions in the physical domain, i.e. find the inversion of the integrals in Eqs. (28) and (29), which can be done by using the Cagniard–de Hoop scheme (Cagniard, 1962; de Hoop, 1960).

4.1. Case (1) and case (2): $c^e_{sh}\geqslant c^m_{sh}$

The original Bromwich path is replaced by a deformed Cagniard contour such that the one-sided Laplace transform can be obtained by inspection. The particular integral contours are chose in the ξ-plane, as shown in Fig. 2. The exponentials in each integral of Eqs. (28) and (29) are taken as the form exp(-pt). In the PE space, we let

$$\alpha^e(\xi)y-\xi x=t. \tag{71}$$

Consequently, the first set of deformed paths are obtained as

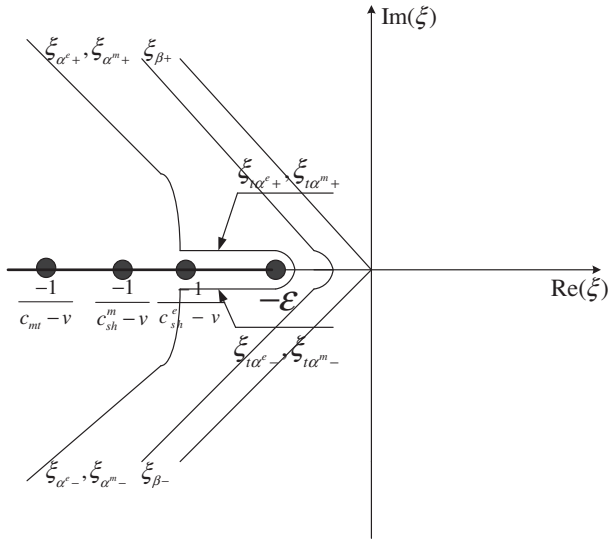

Fig. 2. Cagniard–de Hoop contours in complex plane.

$$\xi_{\alpha^e\pm}=\frac{1}{x^2+\lambda_e^2y^2}\left(-\left(tx+\frac{v}{c^{e2}_{sh}}y^2\right)\pm iy\sqrt{\lambda_e^2t^2-\frac{2v}{c^{e2}_{sh}}xt-\frac{r^2}{c^{e2}_{sh}}}\right),$$
$$r^2=x^2+y^2. \tag{72}$$

The inversion path $\xi_{\alpha^e\pm}$ intercepts the Re(ξ) axis at the location

$$\xi_{\alpha^e}=-\frac{1}{\lambda_e^2c^e_{sh}}\left(\frac{v}{c^e_{sh}}+\frac{x}{\sqrt{x^2+\lambda_e^2y^2}}\right),t_{\alpha^e}=\frac{1}{\lambda_e^2}\left(\frac{vx}{c^{e2}_{sh}}+\frac{\sqrt{x^2+\lambda_e^2y^2}}{c^e_{sh}}\right). \tag{73}$$

It can be verified that $\xi_{\alpha^e}\in(-1/(c^e_{sh}-v),1/(c^e_{sh}+v))$.

As shown in Fig. 2, through the branch cut, the path $\xi_{\alpha^e\pm}$ intercepts the Re(ξ) axis. So a supplemental path $\xi_{t\alpha^e}$ may be needed consisting of two straight segments and a circle of radius R ($R\to 0$) centered at $\xi=-\varepsilon$. The two segments are given as:

$$\xi_{t\alpha^e\pm}=\frac{1}{x^2+\lambda_e^2y^2}\left(-\left(tx+\frac{v}{c^{e2}_{sh}}y^2\right)+y\sqrt{\frac{2v}{c^{e2}_{sh}}xt+\frac{r^2}{c^{e2}_{sh}}-\lambda_e^2t^2}\right)\pm iR, \tag{74}$$

where the range of t satisfy: $t_{\alpha^e0}\leqslant t\leqslant t_{\alpha^e}$, $t_{\alpha^e0}=y/c^e_{sh}$.

Similarly, the second set of the deformed paths are given by

$$\beta^e(\xi)y-\xi x=0, \tag{75}$$

$$\xi_{\beta^e\pm}=\frac{1}{r^2}\left(-xt\pm iyt\sqrt{1-\varepsilon^2\left(\frac{r}{t}\right)^2}\right). \tag{76}$$

The inversion path $\xi_{\beta^e\pm}$ intercepts the Re(ξ) axis at the location

$$\xi_{\beta^e}=-\varepsilon\frac{x}{r},\quad t_{\beta^e}=\varepsilon r. \tag{77}$$

It can be verified that $\xi_{\beta^e}\in(-\varepsilon,\varepsilon)$.

On the other hand, the two set of integration contours can also be achieved in the PM space

$$-\alpha^m(\xi)y-\xi x=t, \tag{78}$$

$$\xi_{\alpha^m\pm}=\frac{1}{x^2+\lambda_m^2y^2}\left(-\left(tx+\frac{v}{c^{m2}_{sh}}y^2\right)\pm iy\sqrt{\lambda_m^2t^2-\frac{2v}{c^{m2}_{sh}}xt-\frac{r^2}{c^{m2}_{sh}}}\right),$$
$$r^2=x^2+y^2. \tag{79}$$

The inversion path $\xi_{\alpha^m\pm}$ intercepts the Re(ξ) axis at the location:

$$\xi_{\alpha^m} = -\frac{1}{\lambda_m^2 c_{sh}^m}\left(\frac{v}{c_{sh}^m} + \frac{x}{\sqrt{x^2+\lambda_m^2 y^2}}\right),$$
$$t_{\alpha^m} = \frac{1}{\lambda^{m2}}\left(\frac{vx}{c_{sh}^{m2}} + \frac{\sqrt{x^2+\lambda_m^2 y^2}}{c_{sh}^m}\right), \tag{80}$$

It can be verified that $\xi_{\alpha^m} \in (-1/(c_{sh}^m - v), 1/(c_{sh}^m + v))$.

For the final integration path, let

$$-\beta^m(\xi)y - \xi x = t \tag{81}$$

$$\xi_{\beta^m} = \xi_{\beta^e} = -\varepsilon\frac{x}{r} \tag{82}$$

The manipulation process is identical to preceding integration paths and can be obtained also.

After having carried out the inversion integrals along the Cagniard–de Hoop contours, then the closed form solutions in the PE half space can be represented by

$$\begin{aligned}
u_3^e(x,y,t) &= \frac{1}{\pi}\int_{t_{\alpha^e}}^{t} \mathrm{Im}\left[A^e(\xi_{\alpha^e+}(\tau))\frac{\partial \xi_{\alpha^e+}(\tau)}{\partial \tau}\right]d\tau,\\
\Phi^e(x,y,t) &= -\frac{1}{\pi}\frac{e_{15}}{\varepsilon_{11}^e}\int_{t_{\beta^e}}^{t} \mathrm{Im}\left[A^e(\xi_{\beta^e+}(\tau))\frac{\partial \xi_{\beta^e+}(\tau)}{\partial \tau}\right]d\tau,\\
\sigma_{yz}^e(x,y,t) &= -\frac{\bar{c}_{44}^e}{\pi}H(t-t_{\alpha^e})\mathrm{Im}\left[\alpha^e(\xi_{\alpha^e+})A^e(\xi_{\alpha^e+})\frac{\partial \xi_{\alpha^e+}}{\partial t}\right]\\
&\quad + \frac{\bar{c}_{44}^e}{\pi}k_e^2 H(t-t_{\beta^e})\mathrm{Im}\left[\beta^e(\xi_{\beta^e+})A^e(\xi_{\beta^e+})\frac{\partial \xi_{\beta^e+}}{\partial t}\right],\\
D_y^e(x,y,t) &= -\frac{e_{15}}{\pi}H(t-t_{\beta^e})\mathrm{Im}\left[\beta^e(\xi_{\beta^e+})A^e(\xi_{\beta^e+})\frac{\partial \xi_{\beta^e+}}{\partial t}\right].
\end{aligned} \tag{83}$$

Similarly, the closed form solutions in the PM half space are also given by

$$\begin{aligned}
u_3^m(x,y,t) &= -\frac{1}{\pi}\int_{t_{\alpha^m}}^{t} \mathrm{Im}\left[A^m(\xi_{\alpha^m+}(\tau))\frac{\partial \xi_{\alpha^m+}(\tau)}{\partial \tau}\right]d\tau,\\
\Psi^m(x,y,t) &= \frac{1}{\pi}\frac{h_{15}}{\mu_{11}^m}\int_{t_{\beta^m}}^{t} \mathrm{Im}\left[A^m(\xi_{\beta^m+}(\tau))\frac{\partial \xi_{\beta^m+}(\tau)}{\partial \tau}\right]d\tau,\\
\sigma_{yz}^m(x,y,t) &= -\frac{\bar{c}_{44}^m}{\pi}H(t-t_{\alpha^m})\mathrm{Im}\left[\alpha^m(\xi_{\alpha^m+})A^m(\xi_{\alpha^m+})\frac{\partial \xi_{\alpha^m+}}{\partial t}\right]\\
&\quad + \frac{\bar{c}_{44}^m}{\pi}k_m^2 H(t-t_{\beta^m})\mathrm{Im}\left[\beta^m(\xi_{\beta^m+})A^m(\xi_{\beta^m+})\frac{\partial \xi_{\beta^m+}}{\partial t}\right],\\
B_y^m(x,y,t) &= -\frac{h_{15}}{\pi}H(t-t_{\beta^m})\mathrm{Im}\left[\beta^m(\xi_{\beta^m+})A^m(\xi_{\beta^m+})\frac{\partial \xi_{\beta^m+}}{\partial t}\right].
\end{aligned} \tag{84}$$

When the PE and PM coupling effects vanish and the media in the upper and lower half spaces are identical, the above solutions degenerate into those for the mode III crack propagating in pure elastic material (Ma and Chen, 1992).

For the crack propagation problem considered in this paper, one of our main concerns is the behavior of the solutions near the crack tip. When $y = 0$, the inversion contours are changed into $\xi_{\alpha+} = \xi_{\beta+} = \xi_+$, and that:

$$\begin{cases} \xi_+ = -\frac{t}{x}, \\ \frac{\partial \xi_+}{\partial t} = -\frac{1}{x}. \end{cases} \tag{85}$$

By setting $x \to 0^+(\varepsilon \to 0)$ the fundamental solutions ahead of the moving crack tip become

$$\begin{aligned}
\sigma_{yz}^i(x,0^+,t) &= \frac{1}{\pi}\frac{c(c_{bg}^e - v)(c_{bg}^m - v)}{v(t+x/v)c_{bg}^e c_{bg}^m (c-v)}\sqrt{\frac{vc_{sh}^e}{(c_{sh}^e - v)}}\\
&\quad \times \frac{(t-x/(c_{bg}^e - v))(t-x/(c_{bg}^m - v))}{(t-x/(c-v))\sqrt{(t-x/(c_{sh}^e - v))}}\frac{F_+(-t/x)}{F_+(1/v)\sqrt{x}}, \quad t > t_{\alpha^i},\\
D_y^e(x,0^+,t) &= \frac{1}{\pi}\frac{e_{15}}{\bar{c}_{44}^e}\frac{c(c_{bg}^e - v)(c_{bg}^m - v)}{(\lambda_e\sqrt{(t-x/(c_{sh}^e - v))(t+x/(c_{sh}^e + v))} - k_e^2 t)}\sqrt{\frac{vc_{sh}^e}{(c_{sh}^e - v)}}\\
&\quad \times \frac{t}{v(t+x/v)c_{bg}^e c_{bg}^m (c-v)}\cdot\frac{(t-x/(c_{bg}^e - v))(t-x/(c_{bg}^m - v))}{(t-x/(c-v))\sqrt{(t-x/(c_{sh}^e - v))}}\frac{F_+(-t/x)}{F_+(1/v)\sqrt{x}}, \quad t > t_{\beta^e},\\
B_y^m(x,0^-,t) &= \frac{1}{\pi}\frac{h_{15}}{\bar{c}_{44}^m}\frac{c(c_{bg}^e - v)(c_{bg}^m - v)}{(\lambda_m\sqrt{(t-x/(c_{sh}^m - v))(t+x/(c_{sh}^m + v))} - k_m^2 t)}\sqrt{\frac{vc_{sh}^e}{(c_{sh}^e - v)}}\\
&\quad \times \frac{t}{v(t+x/v)c_{bg}^e c_{bg}^m (c-v)}\cdot\frac{(t-x/(c_{bg}^e - v))(t-x/(c_{bg}^m - v))}{(t-x/(c-v))\sqrt{(t-x/(c_{sh}^e - v))}}\frac{F_+(-t/x)}{F_+(1/v)\sqrt{x}}, \quad t > t_{\beta^m}.
\end{aligned} \tag{86}$$

When $x \to 0^+$, $t/x \to \infty$, $F_+(-t/x) \to 1$, the asymptotic solutions of the stress, normal electric displacement and magnetic induction ahead of the moving crack tip reduce to

$$\sigma_{yz}(x,0^+,t) \sim \frac{1}{\pi}\cdot\frac{c(c_{bg}^e - v)(c_{bg}^m - v)}{vc_{bg}^e c_{bg}^m (c-v)}\sqrt{\frac{vc_{sh}^e}{(c_{sh}^e - v)}}\frac{1}{\sqrt{tx}}\frac{1}{F_+(1/v)} + o(1), \tag{87}$$

$$D_y(x,0^+,t) \sim \frac{1}{\pi}\frac{e_{15}}{\bar{c}_{44}^e}\frac{1}{(\lambda_e - k_e^2)}\frac{c(c_{bg}^e - v)(c_{bg}^m - v)}{vc_{bg}^e c_{bg}^m (c-v)}\sqrt{\frac{vc_{sh}^e}{(c_{sh}^e - v)}} \times \frac{1}{\sqrt{tx}}\frac{1}{F_+(1/v)} + o(1), \tag{88}$$

$$B_y(x,0^-,t) \sim \frac{1}{\pi}\frac{h_{15}}{\bar{c}_{44}^m}\frac{1}{(\lambda_e - k_m^2)}\frac{c(c_{bg}^e - v)(c_{bg}^m - v)}{vc_{bg}^e c_{bg}^m (c-v)}\sqrt{\frac{vc_{sh}^e}{(c_{sh}^e - v)}} \times \frac{1}{\sqrt{tx}}\frac{1}{F_+(1/v)} + o(1). \tag{89}$$

It can be found from Eqs. (87)–(89) that the stress, electric displacement and magnetic induction exhibit the traditionally square root singularity.

4.2. Case (3) and Case (4): $c_{sh}^e \leqslant c_{sh}^m$

Similarly, we shall derive the explicit solutions in the physical domain for case (3) and (4), which can be done by using the Cagniard–de Hoop scheme. And the asymptotic solutions of the stress, normal electric displacement and magnetic induction ahead of the moving crack tip reduce to

$$\sigma_{yz}(x,0^+,t) \sim \frac{1}{\pi}\cdot\frac{c(c_{bg}^e - v)(c_{bg}^m - v)}{vc_{bg}^e c_{bg}^m (c-v)}\sqrt{\frac{vc_{sh}^m}{(c_{sh}^m - v)}}\frac{1}{\sqrt{tx}}\frac{1}{F_+(1/v)} + o(1), \tag{90}$$

$$D_y(x,0^+,t) \sim \frac{1}{\pi}\frac{e_{15}}{\bar{c}_{44}^e}\frac{1}{(\lambda_e - k_e^2)}\frac{c(c_{bg}^{e-v})(c_{bg}^{m-v})}{vc_{bg}^e c_{bg}^m (c-v)}\sqrt{\frac{vc_{sh}^m}{(c_{sh}^{m-v})}}\frac{1}{\sqrt{tx}}\frac{1}{F_+(1/v)} + o(1), \tag{91}$$

$$B_y(x,0^-,t) \sim \frac{1}{\pi}\frac{h_{15}}{\bar{c}_{44}^m}\frac{1}{(\lambda_e - k_m^2)}\frac{c(c_{bg}^{e-v})(c_{bg}^{m-v})}{vc_{bg}^e c_{bg}^m (c-v)}\sqrt{\frac{vc_{sh}^m}{(c_{sh}^{m-v})}}\frac{1}{\sqrt{tx}}\frac{1}{F_+(1/v)} + o(1). \tag{92}$$

It can be found from Eqs. (90)–(92) that the stress, electric displacement and magnetic induction exhibit the traditionally square root singularity.

5. Dynamic intensity factors and energy release rate (ERR)

In Section 4, the fundamental solutions under a pair of the concentrated loads have been derived. Next, we shall employ these fundamental solutions to obtain the dynamic intensity factors of the stress, electric displacement and magnetic induction as well as the dynamic ERR for a general distributed load. The intensity factors and ERR is of importance for understanding the fracture behaviors of MEE solids.

5.1. Case (1) and Case (2): $c^e_{sh} \geqslant c^m_{sh}$

Assume that the newly formed crack surfaces ($0 < x < vt$) are subjected to a general anti-symmetric external load distribution. According to the superposing principle, the general field solutions ahead of the crack are represented by

$$\begin{aligned}
\sigma^{(q)}(x,t) &= \int_0^{vt} \sigma_{yz}(x,0,t-X/v)p(X)dX,\\
D_y^{(q)}(x,t) &= \int_0^{vt} D_y(x,0,t-X/v)p(X)dX,\\
B_y^{(q)}(x,t) &= \int_0^{vt} B_y(x,0,t-X/v)p(X)dX,
\end{aligned} \tag{93}$$

where the superscript (q) denotes the field quantities induced by the general traction load distribution.

Making the change of variable $vt - X = \eta$ and letting

$$P(l) \triangleq \sqrt{\frac{2}{\pi}} \int_0^l \eta^{-1/2} p(l-\eta)d\eta, \tag{94}$$

Then the dynamic stress, electric displacement and magnetic induction intensity factors for this general load distribution are

$$\begin{aligned}
K^{(\sigma)}_{IIIT}(vt,v) &= \lim_{x\to 0}\sqrt{2\pi x}\sigma^{(q)}(x,t)\\
&= \frac{c(c^e_{bg}-v)(c^m_{bg}-v)}{c^e_{bg}c^m_{bg}(c-v)}\sqrt{\frac{c^e_{sh}}{(c^e_{sh}-v)}}\frac{1}{F_+(1/v)}P(vt),
\end{aligned} \tag{95}$$

$$\begin{aligned}
K^{(D)}_{IIIT}(vt,v) &= \lim_{x\to 0}\sqrt{2\pi x}D_y^{(q)}(x,t) = \frac{\varepsilon^e_{11}}{e_{15}}\frac{k_e^2}{(\lambda_e-k_e^2)}\frac{c(c^e_{bg}-v)(c^m_{bg}-v)}{c^e_{bg}c^m_{bg}(c-v)}\\
&\times\sqrt{\frac{c^e_{sh}}{(c^e_{sh}-v)}}\frac{1}{F_+(1/v)}P(vt),
\end{aligned} \tag{96}$$

$$\begin{aligned}
K^{(B)}_{IIIT}(vt,v) &= \lim_{x\to 0}\sqrt{2\pi x}B_y^{(q)}(x,t) = \frac{\mu^m_{11}}{h_{15}}\frac{k_m^2}{(\lambda_m-k_m^2)}\frac{c(c^e_{bg}-v)(c^m_{bg}-v)}{c^e_{bg}c^m_{bg}(c-v)}\\
&\times\sqrt{\frac{c^e_{sh}}{(c^e_{sh}-v)}}\frac{1}{F_+(1/v)}P(vt).
\end{aligned} \tag{97}$$

It is convenient to introduce a normalization based on the corresponding "quasi-static" intensity factors, as shown by Freund (1972) for the crack propagation problem in a purely elastic material. The relevant intensity factors are

$$\begin{aligned}
K^{(\sigma)}_{IIIT}(vt,0) &= P(vt),\\
K^{(D)}_{IIIT}(vt,0) &= \frac{\varepsilon^e_{11}}{e_{15}}\frac{k_e^2}{1-k_e^2}P(vt),\\
K^{(B)}_{IIIT}(vt,0) &= \frac{\mu^m_{11}}{h_{15}}\frac{k_m^2}{1-k_m^2}P(vt).
\end{aligned} \tag{98}$$

By defining

$$\begin{aligned}
f(v) &\triangleq \frac{c(c^e_{bg}-v)(c^m_{bg}-v)}{c^e_{bg}c^m_{bg}(c-v)}\sqrt{\frac{c^e_{sh}}{(c^e_{sh}-v)}}\frac{1}{F_+(1/v)},\\
g(v) &\triangleq \frac{1-k_e^2}{\lambda_e-k_e^2}f(v),\\
h(v) &\triangleq \frac{1-k_m^2}{\lambda_m-k_m^2}f(v).
\end{aligned} \tag{99}$$

The dynamic intensity factors of stress, electric displacement and magnetic induction can be written as the following simple forms

$$\begin{aligned}
K^{(\sigma)}_{IIIT}(vt,v) &= f(v)K^{(\sigma)}_{IIIT}(vt,0),\\
K^{(D)}_{IIIT}(vt,v) &= g(v)K^{(D)}_{IIIT}(vt,0),\\
K^{(B)}_{IIIT}(vt,v) &= h(v)K^{(B)}_{IIIT}(vt,0).
\end{aligned} \tag{100}$$

From Eq. (99), it is seen that $f(v)$, $g(v)$ and $h(v)$ depend on crack speed, the material properties and the velocities of three different kinds of the waves, which are the bulk shear wave, the generalized B–G wave and generalized M–T interfacial wave. They are independent of the crack extension length vt and the load distribution function $P(x)$. Consequently, $f(v)$, $g(v)$ and $h(v)$ can be regarded as the universal functions of the dynamic interfacial propagation in PE/PM bi-materials.

Atkinson and Eshelby (1968) obtained the dynamic energy release rate for the purely elastic material. The static ERR for the MEE solid is first derived by Wang and Mai (2003) based on the virtual crack closure integral method. In a way analogous to the PE case, the dynamic ERR for the interfacial running crack considered in this paper can be calculated by

$$\begin{aligned}
G(vt,v) &= \lim_{\Gamma\to 0}\int_\Gamma \left[\sigma^e_{yz}(x,0,t)\frac{\partial u^e_3}{\partial x}(x,0,t) + D^e_y(x,0,t)\frac{\partial \phi^e}{\partial x}(x,0,t)\right]dx\\
&\quad + \lim_{\Gamma\to 0}\int_\Gamma vEn_1\,d\Gamma\\
&= \lim_{l\to 0}\int_{-l}^{l}\left[\sigma^e_{yz}(x,0,t)\frac{\partial u^e_3}{\partial x}(x,0,t) + D^e_y(x,0,t)\frac{\partial \phi^e}{\partial x}(x,0,t)\right]dx\\
&\quad - \lim_{l\to 0}\int_{l}^{-l}\left[\sigma^m_{yz}(x,0,t)\frac{\partial u^m_3}{\partial x}(x,0,t) + B^m_y(x,0,t)\frac{\partial \psi^m}{\partial x}(x,0,t)\right]dx,
\end{aligned} \tag{101}$$

where Γ is the contour surrounding the crack tip, and alone the segment parallel to the crack surface $n_1 = 0$. E is the total energy density made up of the kinetic energy density and internal energy density.

Since the electric potential and magnetic potential are zero both along the line ahead of the crack and on the crack faces; consequently, there is no contribution from electric field and magnetic field to the dynamic free energy release rate, and therefore, the free-energy release rate is the same as the purely mechanical ERR. Therefore, Eq. (101) reduces to

$$G(vt,v) = \lim_{l\to 0}\int_{-l}^{l}\left[\sigma^e_{yz}(x,0,t)\frac{\partial u^e_3}{\partial x}(x,0,t) + \sigma^m_{yz}(x,0,t)\frac{\partial u^m_3}{\partial x}(x,0,t)\right]dx \tag{102}$$

Making use of the identity

$$\lim_{l\to 0}\int_{-l}^{l}\left[\frac{H(x)}{\sqrt{x}} + \frac{H(-x)}{\sqrt{-x}}\right]dx = \frac{\pi}{2}, \tag{103}$$

One can obtain

$$G(vt,v) = \frac{1}{4}\frac{\bar{c}^e_{44}(\lambda_e-k_e^2)+\bar{c}^m_{44}(\lambda_m-k_m^2)}{\bar{c}^e_{44}(\lambda_e-k_e^2)\bar{c}^m_{44}(\lambda_m-k_m^2)}[K^{(\sigma)}_{IIIT}(vt,v)]^2. \tag{104}$$

Table 2
Material properties used in the calculations.

	$BaTiO_3$	PZT-7	PZT-4	$CoFe_2O_4$
c_{44} ($\times 10^9$ N/m^2)	43.9	25	25.6	45.3
e_{15} (C/m^2)	11.4	13.5	12.7	–
h_{15}(N/A m)	–	–	–	550
ε_{11}($\times 10^{-9}$ C^2/N m)	9.82	17.1	6.46	–
μ_{11} ($\times 10^{-6}$ N S^2/C^2)	–	–	–	157
ρ (10^3 kg/m^3)	5.7	7.8	7.5	5.3
c_{sh} ($\times 10^3$ m/s)	3.166	2.138	2.596	2.985

Table 3
Three cases corresponding to different bi-material combinations.

bi-materials	$c^e_{bg} \vee c^m_{bg}$	k_e/k_m	c_{mt} ($\times 10^3$ m/s)	Cases
$BaTiO_3/CoFe_2O_4$	>	2.38	–	(2)
PZT-4/$CoFe_2O_4$	<	3.48	2.591	(3)
PZT-7/$CoFe_2O_4$	<	1.87	–	(4)

According to the relevant quasi-static elastic solution,

$$G(vt,0)=\frac{1}{4}\frac{\bar{c}^e_{44}(1-k_e^2)+\bar{c}^m_{44}(1-k_m^2)}{\bar{c}^e_{44}(1-k_e^2)\bar{c}^m_{44}(1-k_m^2)}(P(vt))^2. \tag{105}$$

Then the normalized energy release rate can be obtained:

$$\begin{aligned}\frac{G(vt,v)}{G(vt,0)}&=\frac{\bar{c}^e_{44}(\lambda_e-k_e^2)+\bar{c}^m_{44}(\lambda_m-k_m^2)}{(\lambda_e-k_e^2)(\lambda_m-k_m^2)}\\&\times\frac{(1-k_e^2)(1-k_m^2)}{\bar{c}^e_{44}(1-k_e^2)+\bar{c}^m_{44}(1-k_m^2)}\\&\times\frac{c^2(c^e_{bg}-v)^2(c^m_{bg}-v)^2}{c^{e2}_{bg}c^{m2}_{bg}(c-v)^2}\frac{c^e_{sh}}{c^e_{sh}-v}\frac{1}{(F_+(1/v))^2}\end{aligned} \tag{106}$$

Note that when $k_m = 0$, the solution degenerates to one of a dynamic mode III interfacial crack propagation in an elastic–piezoelectric bi-material by Chen et al. (2008). When $k_e = 0.00$, the solution degenerates to the case of an elastic–PM bi-material containing a semi-infinite crack along the interface.

5.2. Case (3) and case (4): $c^e_{sh} \leqslant c^m_{sh}$

Similarly, the dynamic intensity factors of stress, electric displacement and magnetic induction as well as energy release rate (ERR) for case (3) and (4) are obtained in explicit forms:

$$\begin{aligned}f(v)&\triangleq\frac{c(c^e_{bg}-v)(c^m_{bg}-v)}{c^e_{bg}c^m_{bg}(c-v)}\sqrt{\frac{c^m_{sh}}{(c^m_{sh}-v)}}\frac{1}{F_+(1/v)},\\g(v)&\triangleq\frac{1-k_e^2}{\lambda_e-k_e^2}f(v),\\h(v)&\triangleq\frac{1-k_m^2}{\lambda_m-k_m^2}f(v).\end{aligned} \tag{107}$$

and

$$\begin{aligned}\frac{G(vt,v)}{G(vt,0)}&=\frac{\bar{c}^e_{44}(\lambda_e-k_e^2)+\bar{c}^m_{44}(\lambda_m-k_m^2)}{(\lambda_e-k_e^2)(\lambda_m-k_m^2)}\\&\times\frac{(1-k_e^2)(1-k_m^2)}{\bar{c}^e_{44}(1-k_e^2)+\bar{c}^m_{44}(1-k_m^2)}\\&\times\frac{c^2(c^e_{bg}-v)^2(c^m_{bg}-v)^2}{c^{e2}_{bg}c^{m2}_{bg}(c-v)^2}\frac{c^m_{sh}}{c^m_{sh}-v}\frac{1}{(F_+(1/v))^2}.\end{aligned} \tag{108}$$

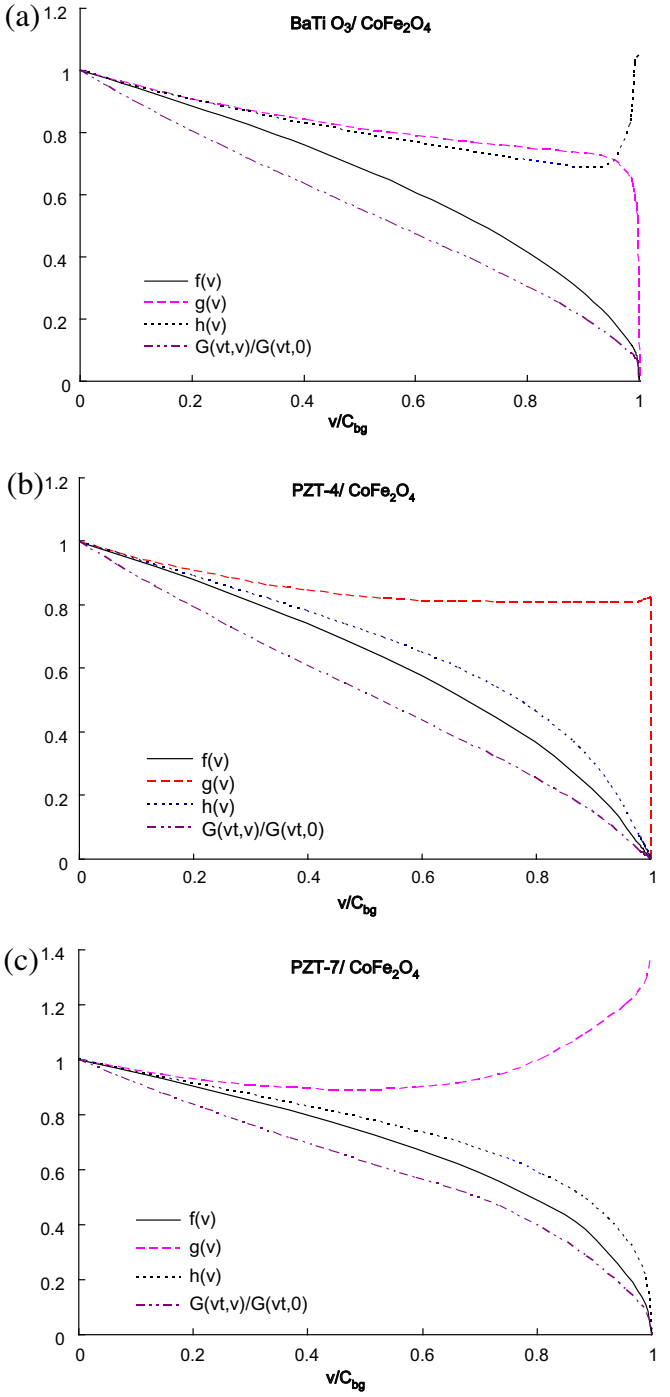

Fig. 3. Variations of the universal function $f(v)$, $g(v)$, $h(v)$ and the dimensionless dynamic ERR $G(vt,v)/G(vt,0)$ versus the dimensionless velocity v/c_{bg} for the following bi-materials: (a) $BaTiO_3/CoFe_2O_4$; (b) PZT-4/$CoFe_2O_4$; (c) PZT-7/$CoFe_2O_4$.

6. Numerical examples

Based on the explicit transient solution obtained in the previous section, the numerical results for the universal functions and the dimensionless dynamic ERR are presented for several different material combinations. In our calculation, the PE materials are $BaTiO_3$, PZT-4 and PZT-7, respectively, while the PM material is $CoFe_2O_4$. The material constants of these materials and the corresponding bulk shear wave velocities are listed in Table 2. They

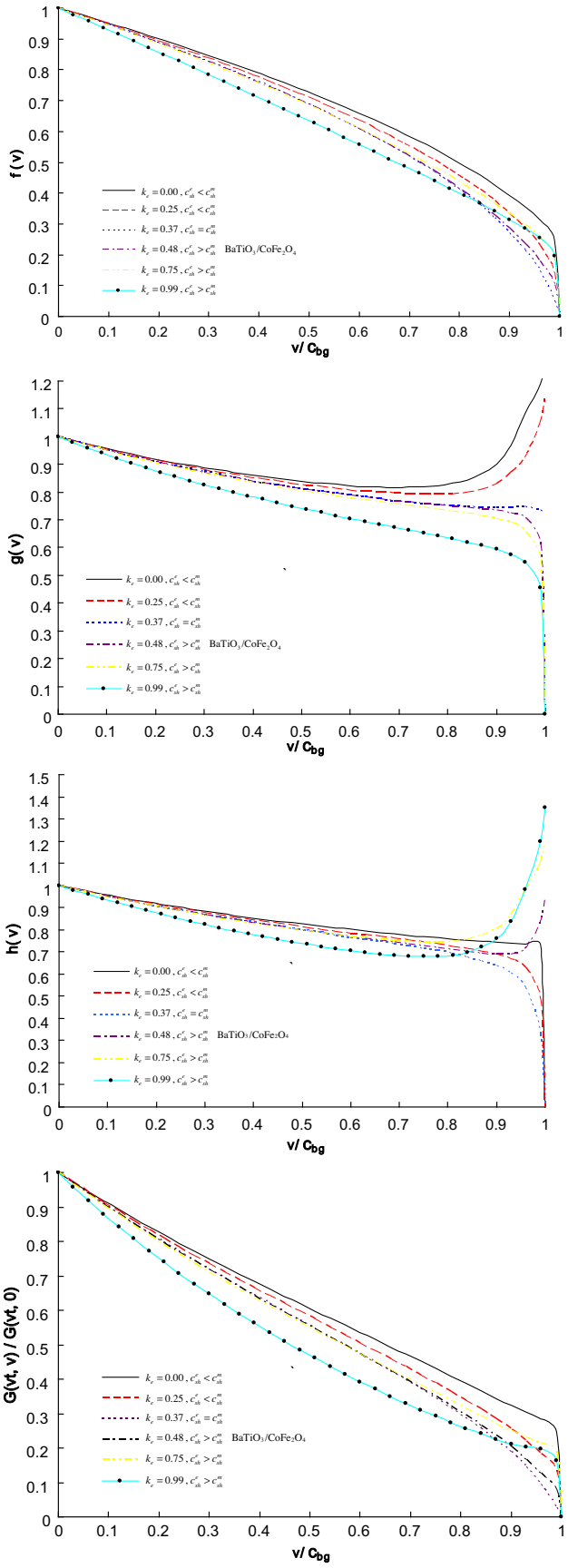

Fig. 4. Variations of the universal functions and the dimensionless ERR versus the dimensionless velocity v/c_{bg} for a broad range of electro-mechanical coupling coefficient (k_e = 0.00, 0.25, 0.37, 0.48, 0.75, 0.99).

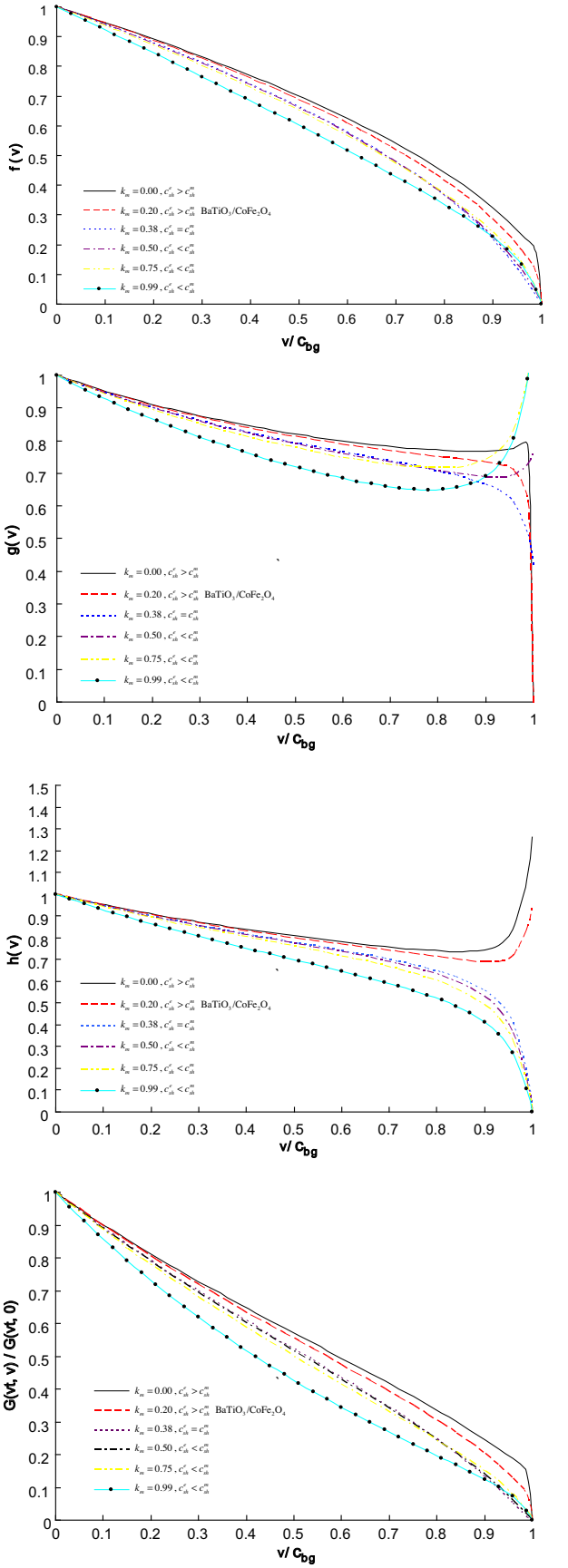

Fig. 5. Variations of the universal functions and the dimensionless ERR versus the dimensionless velocity v/c_{bg} for a broad range of magneto-mechanical coupling coefficient (k_m = 0.00, 0.25, 0.5, 0.74, 0.92, 0.99).

can be found in Jiang et al. (2006) and Liu et al. (2008). Three kinds of the bi-materials combining $CoFe_2O_4$ with $BaTiO_3$, PZT-4 and PZT-7 correspond to three different cases correspond to three cases analyzed in the previous section (see Table 3).

Fig. 3 shows the variation of the universal functions and the dimensionless dynamic ERR with the normalized crack propagation speed v/c_{bg} for three different bi–materials, where $c_{bg} = \min(c^e_{bg}, c^m_{bg})$ is the slower B-G wave speed. From Fig. 3, it can seen that the universal function $f(v)$ of stress intensity factor and the dimensionless dynamic ERR $G(vt,v)/G(vt,0)$ decrease monotonously with increasing crack propagation velocity v and vanish when v reaches c_{bg}. This means that the slower B–G wave speed is the limiting velocity of the interfacial propagation. The variation of the universal functions $g(v)$ and $h(v)$ depend on the relations between c^e_{bg} and c^m_{bg}. When $c^e_{bg} > c^m_{bg}$, i.e. for the $BaTiO_3/CoFe_2O_4$ bi-material, $g(v)$ decreases as v/c_{bg} increases and trends towards zero, while $h(v)$ first reduces gradually and then reach its maximum. For the PZT-4/$CoFe_2O_4$ and PZT-7/$CoFe_2O_4$ bi-materials, where $c^e_{bg} < c^m_{bg}$, the variations of $g(v)$ and $h(v)$ are similar to those of $h(v)$ and $g(v)$ of the $BaTiO_3/CoFe_2O_4$ bi-material, respectively.

In the second example, we consider a PE half space overlying the $CoFe_2O_4$ half-space with $k_m = 0.2$, where the electro-mechanical coupling coefficient k_e of the PE half space is allowed to change while other material constants are the same as the $BaTiO_3$. Fig. 4 plots the universal functions and the dimensionless ERR for a broad range of electro-mechanical coupling coefficient ($k_e = 0.00$, 0.25, 0.37, 0.48, 0.75, 0.99) against the dimensionless velocity v/c_{bg}. When $0 \leqslant k_e < 0.37$, the bulk shear wave speed in a PE medium is slower than that in a PM medium. When $0.34 \leqslant k_e \leqslant 0.41$, the generalized M–T wave exists, which corresponds to the case (1) analyzed in the previous section. The universal functions $f(v)$ and $G(vt,v)/G(vt,0)$ decreases smoothly with increasing crack propagation velocity v and reaches zero when v reaches c_{bg}. And the universal functions $g(v)$ and $h(v)$ are more complicated and do not necessarily decrease to zero when the crack speed reaches the slower B–G wave speed.

Finally, we examine the bi-material consisting of the $BaTiO_3$ half-space with $k_e = 0.55$ and a PM half space whose magneto-mechanical coupling coefficient k_m is allowed to vary in a very broad range. Other material properties of the PM half are chosen to be the same as the $CoFe_2O_4$. Fig. 5 plots the universal functions and the dimensionless ERR for various magneto-mechanical coupling coefficient ($k_m = 0.00$, 0.20, 0.38, 0.50, 0.75, 0.99) versus the dimensionless velocity v/c_{bg}. When $0 \leqslant k_m < 0.92$, the bulk shear wave speed in a PE medium is faster than that in a PM medium. The universal functions $f(v)$ and $G(vt,v)/G(vt,0)$ decreases smoothly with increasing crack propagation velocity v and reaches zero when v reaches c_{bg}. The universal functions $g(v)$ and $h(v)$ are more complicated and show the same tendency as the second example.

7. Conclusions

The dynamic fracture problem of a mode-III crack running along the interface in a PE–PM bi-material is studied. The problem becomes interesting and complicated when the B–G waves and the generalized M–T waves propagating along the interface are taken into consideration. Different from the moving crack problems reported in the literatures, the numerical results of the present paper show that the dimensionless stress intensity and energy release rate always vanish when the crack propagation velocity arrives at the slower B–G wave velocity in both materials. This means that the B–G waves play an important role in determining the dynamic fracture characteristics of PE/PM composites.

Acknowledgements

The authors are grateful for the support by National Natural Science Foundation of China under Grants #11090330, #11090331 and #11072003. Support by the National Basic Research Program of China (#G2010CB832701) is also acknowledged.

References

Atkinson, C., Eshelby, J.D., 1968. The flow of energy into the tip of a moving crack. Int. J. Fract. Mech. 4, 3–8.
Bichurin, M.I., Petrov, V.M., Srinivasan, G., 2003. Theory of low-frequency magnetoelectric coupling in magnetostrictive-piezoelectric bilayers. Phys. Rev. B 68 (5), 054402.
Cagniard, L., 1939. Reflexion et Refraction des Ondes Seismiques Progressives. Gauthier-Villars, Paris. English translation: Reflection and Refraction of Progressive Seismic Waves. Flinn, E.A., Dix, C.H., 1962, McGraw-Hill, New York.
Chen, X.H., Ma, C.C., Ing, Y.S., Tsai, C.H., 2008. Dynamic interfacial crackpropagation in elastic–piezoelectric bi-materials subjected to uniformly distributed loading. Int. J. Solids Struct. 45, 959–997.
Chen, X.H., 2009a. Energy release rate and path-independent integral in dynamic fracture of magneto-electro-thermo-elastic solids. Int. J. Solids Struct. 46, 2706–2711.
Chen, X.H., 2009b. Dynamic crack propagation in a magneto-electro-elastic solid subjected to mixed loads: transient Mode-III problem. Int. J. Solids Struct. 46, 4025–4037.
de Hoop, A.T., 1960. A modification of Cagniard's method for solving seismic pulse problems. Appl. Sci. Res. B. 8, 349–360.
Du, J.K., Shen, Y.P., Ye, D.Y., Yue, F.R., 2004. Scattering of anti-plane shear waves by a partially debonded magneto-electro-elastic circular cylindrical inhomogeneity. Int. J. Eng. Sci. 42, 887–913.
Feng, W.J., Li, Y.S., Xu, Z.H., 2009. Transient response of an interfacial crack between dissimilar magnetoelectroelastic layers under magnetoelectromechanical impact loadings: mode-I problem. Int. J. Solids Struct. 46, 3346–3356.
Feng, W.J., Liu, J.X., 2007. Dynamic analysis of a magneto-electro-elastic material with a semi-infinite mode-III crack under point impact loads. Struct. Eng. Mech. 27, 609–623.
Feng, W.J., Su, R.K.L., 2006. Dynamic internal crack problem of a functionally graded magneto-electro-elastic strip. Int. J. Solids Struct. 43, 5196–5216.
Feng, W.J., Su, R.K.L., Liu, Y.Q., 2006. Scattering of SH waves by an arc-shaped interface crack between a cylindrical magneto-electro-elastic inclusion and matrix with the symmetry of 6 mm. Acta Mech. 183, 81–102.
Feng, W.J., Su, R.K.L., 2007. Dynamic fracture behaviors of cracks in a functionally graded magneto-electro-elastic plate. Eur. J. Mech. A – Solids 26, 363–379.
Feng, W.J., Xue, Y., Zou, Z.Z., 2005. Crack growth of an interface crack between two dissimilar magneto-electro-elastic materials under anti-plane mechanic and in-plane electric magnetic impact. Theor. Appl. Fract. Mech. 43, 376–394.
Freund, L.B., 1972. Crack Propagation in an elastic solid subjected to general loading. I: Constant rate of extension. J. Mech. Phys. Solids 20, 120–140.
Freund, L.B., 1990. Dynamic Fracture Mechanics. Cambridge University Press, Cambridge.
Hu, K.Q., Kang, Y.L., Qin, Q.H., 2007. A moving crack in a rectangular magnetoelectroelastic body. Eng. Fract. Mech. 74, 751–770.
Hu, K.Q., Li, G.Q., 2005. Constant moving crack in a magnetoelectroelastic material under anti-plane shear loading. Int. J. Solids Struct. 42, 2823–2835.
Huang, Y., Li, X.F., Lee, K.Y., 2009. Interfacial shear horizontal (SH) waves propagating in a two-phase piezoelectric/piezomagnetic structure with an imperfect interface. Philos. Mag. Lett. 89, 95–103.
Ing, Y.S., Ma, C.C., 1996. Transient response of a finite crack subjected to dynamic anti-plane loading. Int. J. Fract. 82, 345–362.
Ing, Y.S., Ma, C.C., 1997. Dynamic fracture analysis of a finite crack subjected to an incident horizontally polarized shear wave. Int. J. Solids Struct. 34, 895–910.
Jiang, S.N., Jiang, Q., Li, X.F., 2006. Piezoelectromagnetic waves in a ceramic plate between two ceramic half-spaces. Int. J. Solids Struct. 43, 5799–5810.
Li, S., Mataga, P.A., 1996. Dynamic crack propagation in piezoelectric materials. Part I: Electrode solution. J. Mech. Phys. Solids 44, 1799–1830.
Li, X.F., 2005. Dynamic analysis of a cracked magnetoelectroelastic medium under antiplane mechanical and inplane electric and magnetic impacts. Int. J. Solids Struct. 42, 3185–3205.
Li, Y.D., Lee, K.Y., 2009. Dynamic responses of a crack in a layered graded magnetoelectroelastic sensor subjected to harmonic waves. Acta Mech. 204, 217–234.
Liu, J.X., Fang, D.N., Wei, W.Y., Zhao, X.F., 2008. Love waves in layeredpiezoelectric/piezomagnetic structures. J. Sound Vib. 315, 146–156.
Ma, C.C., Chen, S.K., 1992. Investigation on the stress intensity factor field for unstable dynamic crack growth. Int. J. Fract. 58, 345–359.
Melkumyan, A., Mai, Y.W., 2008. Influence of imperfect bonding on interface waves guided by piezoelectric/piezomagnetic composites. Philos. Mag. 88, 2965–2977.
Nan, C.W., Bichurin, M.I., Dong, S.X., Viehland, D., Srinivasan, G., 2008. Multiferroic magnetoelectric composites: historical perspective, status, and future directions. J. Appl. Phys. 103, 031–101.
Noble, B., 1958. Methods based on the Wiener–Hopf technique. Pergamon Press, New York.

Priya, S., Islam, R., Dong, S.X., Viehland, D., 2007. Recent advancements in magnetoelectric particulate and laminate composites. J. Electroceram. 19, 149–166.

Rangelov, T., Stoynov, Y., Dineva, P., 2011. Dynamic fracture behavior of functionally graded magnetoelectroelastic solids by BIEM. Int. J. Solids Struct. 48, 2987–2999.

Rojas, Diaz R., Garcia, Sanchez F., Saez, A., 2010. Analysis of cracked magnetoelectroelastic composites under time-harmonic loading. Int. J. Solids. Struct. 47, 71–80.

Soh, A.K., Liu, J.X., 2006. Interfacial shear horizontal waves in a piezoelectric-piezomagnetic bi-material. Philos. Mag. Lett. 86, 31–35.

Tupholme, G.E., 2009. Moving antiplane shear crack in transversely isotropic magnetoelectroelastic media. Acta Mech. 202, 153–162.

To, A.C., Li, S.F., Claser, S.D., 2006. Propagation of a mode-III interfacial conductive crack along a conductive interface between two piezoelectric materials. Wave Motion 43, 368–386.

Van Suchtelen, J., 1972. Product properties: a new application of composite materials. Philips Res. Rep. 27, 28–37.

Van den Boomgaard, J., Terrell, D.R., Born, R.A.J., Giller, H.F.J.I., 1974. In situ grown eutectic magnetoelectric composite material. J. Mater. Sci. 9, 1705–1709.

Van den Boomgaard, J., van Run, A.M.J.G., van Suchtelen, J., 1976. Magnetoelectricity in piezoelectric-magnetostrictive composites. Ferroelectrics 10, 295–298.

Wang, B.L., Han, J.C., Du, S.Y., 2010. Transient fracture of a layered magnetoelectroelastic medium. Mech. Mater. 42, 3.

Wang, B.L., Mai, Y.W., 2003. Fracture of piezoelectromagnetic materials. Mech. Res. Commun. 31, 65–73.

Yong, H.D., Zhou, Y.H., 2007. Transient response of a cracked magnetoelectroelastic strip under anti-plane impact. Int. J. Solids Struct. 44, 705–717.

Zhang, P.W., 2011. Dynamic fracture of a rectangular limited-permeable crack in magneto-electro-elastic media under a time-harmonic elastic P-wave. Int. J. Solids Struct. 48 (3–4), 553–566.

Zhong, X.C., Li, X.F., 2006. A finite length crack propagating along the interface of two dissimilar magnetoelectroelastic materials. Int. J. Eng. Sci. 44, 1394–1407.

Zhong, X.C., Li, X.F., Lee, K.Y., 2009. Transient response of a cracked magnetoelectric material under the action of in-plane sudden impacts. Comput. Mater. Sci. 45, 905–911.

Zhou, Z.G., Wang, B., 2006. Dynamic behavior of two parallel symmetry cracks in magneto-electro-elastic composites under harmonic anti-plane waves. Appl. Math. Mech. – Engl. Ed. 27, 583–591.

Zhou, Z.G., Wang, B., 2008. An interface crack between two dissimilar functionally graded piezoelectric/piezomagnetic material half infinite planes subjected to the harmonic anti-plane shear stress waves. Int. J. Appl. Electrom. Mech. 27, 117–132.